

Optical properties of Ga monocrystal in the 0.3–5-eV range

R. Kofman, P. Cheyssac, and J. Richard

Laboratoire d'Electro-optique Laboratoire associé au CNRS L.A. 190 Parc Valrose 06034 Nice-Cedex, France

(Received 12 July 1977)

The optical constants relative to each crystallographic axis of Ga monocrystals in the range 0.3–5 eV have been determined from reflectance measurements at normal incidence with the light being polarized parallel to each axis. We report on thermorefectance spectra and give the corresponding changes in the dielectric constants. The spectra are interpreted in terms of electronic interband and intraband transitions.

I. INTRODUCTION

Discovered in 1875 by Lecoq de Boisbaudran, gallium is the first element isolated after the publication by Mendeleieff of his periodic table. It is characterized by some very particular properties. For example, it has a low melting point (29.7°C), dilates when becoming solid, and is strongly anisotropic (the ratio between its greatest and smallest conductivity is 7, the highest value among all the metals).

Nevertheless its optical properties have not been investigated very much. The actual values of the optical characteristics reported are very different probably due to the nature of the samples investigated. Wesolowska *et al.*^{1,2} have investigated the optical properties of thin Ga films in the visible and near ir and uv. So did Rapp,³ Bor,⁴ Eichis,⁵ while recently, Hunderi and Ryberg⁶ tried to interpret the results concerning specular films evaporated onto substrates held at 80 K with the aid of band calculation. But gallium is anisotropic and its optical properties must be defined by three pairs of constants, one for each axis of the orthorhombic system to which it belongs. Its unit cell, according to Barrett (cf. Slater⁷), holds eight atoms, its dimensions being $a = 4.5151 \text{ \AA}$, $b = 4.4881 \text{ \AA}$, $c = 7.6318 \text{ \AA}$ at 2.35 K. To our knowledge only Lenham^{8,9} and Rapp¹⁰ have tried to determine the values of the optical constants along

each axis. Lenham used polished monocrystals, while Rapp avoided the drawback due to polishing with monocrystals grown from molten gallium poured onto a carefully cleaned flat glass. The method used to determine the optical constants was Beattie's¹¹ where the ratio of the reflectance and phase difference for light polarized parallel and perpendicular to the plane of incidence are measured. This method is very sensitive to the state of the surface which can be seen from Lenham results concerning hand-polished and electro-polished samples.

Our aim was to investigate and understand the optical properties of gallium monocrystals grown by slow crystallization from liquid previously heated to a temperature just above the melting point. The monocrystal grows with a characteristic shape (Fig. 1) with two interesting faces: one (010) in which axes a and c can be found, the other (001) with the axes a and b . Figure 2 shows samples grown with this technique where (001) and (010) faces can be seen.

In Sec. II of this paper the experimental technique and the method used to determine the optical constants will be described. In Sec. III thermorefectance spectra in the range 0.4–5 eV will be

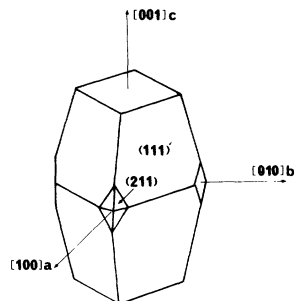


FIG. 1. Shape of an idiomorphic gallium monocrystal.



FIG. 2. Photography of gallium monocrystals.

given: and in Sec. IV we shall try to interpret the results in terms of band structure.

II. DETERMINATION OF THE OPTICAL CONSTANTS

A. Measure of reflectance

Figure 3 represents the apparatus with which the reflectance R at normal incidence is measured. The light source is either a xenon discharge lamp HP XBO (for the visible and near uv), or a quartz iodine lamp (for the visible and near ir). The lamps are provided with dc current from a storage battery. The grating monochromator used is a Jobin et Yvon HRS 2. The light beam after the monochromator is chopped at the frequency $f=26$ Hz by the mirror M_1 and enters the photomultiplier either directly or after being reflected on the sample and mirror M_2 . Both mirrors M_1 and M_2 have been prepared at the same time and have the same reflectance. The light is linearly polarized, after the monochromator, with a Rochon polarizer. The mean angle of incidence onto the sample is about 2° , with a beam aperture of 10^{-2} rad. The angles of incidence onto both mirrors M_1 and M_2 are the same. Both reflected beams arrive at the same point of the photocathode. A slight difference of about 1° , between the angles of incidence of the incident beams entering the photomultiplier, may exist which could cause a gain difference. Such a difficulty has been avoided by setting a silica diffuser in front of the photocathode. The signals given by the photomultiplier are amplified then chopped and shaped by an electric chopper. One output of the chopper gives a signal I proportional to the light intensity received by the photomultiplier after reflection onto mirror M_1 . It is used to control the high-voltage bias of the photomultiplier so

that I stays constant during the measurement. The other output gives a signal RI proportional to the light intensity received by the photomultiplier after reflection by the sample and mirror M_2 . The reflectance R is measured by an ac voltmeter and registered. The error on the measurement of R is about 2%.

Gallium monocrystals are grown by a slowly cooling molten Ga whose purity is 99.999%. During this period gallium surfaces are protected from oxidation by a dilute HCl solution, the unit nesting in a vessel filled with nitrogen. The HCl solution is $N/200$ and is used in order to dissolve gallium oxide which could have happen at the surface of the liquid Ga. The growing monocrystal floats with the optically interesting faces being under the surface of the liquid Ga. A further examination of these faces with a scanning microscope has shown that the defects of the investigated surfaces, if any, are less than 100 \AA in dimension. The samples are then put into an optical cryostat in which vacuum can be maintained. The duration of its handling is very short and during all this time nitrogen flows onto the monocrystal surfaces.

Figure 4 gives the reflectance R , at normal incidence, of the (001) face at different temperatures, light being polarized parallel to axis a , in the range $0.3\text{--}0.9 \mu\text{m}$. Figure 5 gives the reflectance R for the same surface light being polarized parallel to axis b , while Fig. 6 is the normal reflectance of (010) face light polarized parallel to c axis.

B. Determination of the optical constants

We compare, first of all, the method used by Lenham⁸ and Rapp¹⁰ who were the first to work

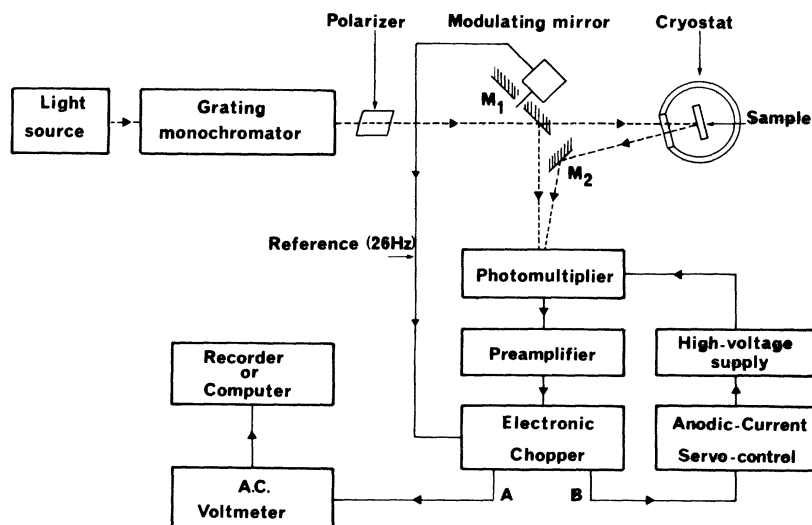


FIG. 3. Scheme of the experimental device.

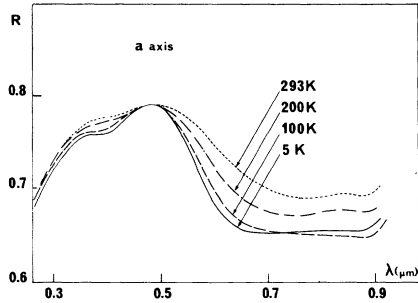


FIG. 4. Reflectance of a (001) surface, light polarized parallel to axis *a*, at different temperatures.

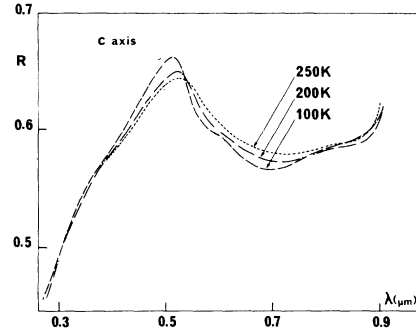


FIG. 6. Reflectance of a (010) surface light polarized parallel to axis *c*, at different temperatures.

with monocrystals. The experimental technique they used is the same. The sample was fixed with one of the crystal axes in the reflecting surface normal to the plane of incidence; the other two axes laid in this plane, one being fixed parallel to the surface normal. Lenham measured the ratio of reflectance for parallel and perpendicular polarized radiation and the cosine of the phase difference Δ . Another series of values of ρ and $\cos\Delta$ is obtained after a rotation of 90° of the sample around the normal to its surface. Using equations derived by Drude¹² for orthorhombic biaxial crystals, calculations were made of the complex refractive indices N_a, N_b, N_c , referring to propagation of a ray with the electric vector vibrating along the respective directions (*a, b, c*) in the crystal. Each complex index can be written as $N = n - jk$. The Drude equations may be written in the form

$$r_y^x = \rho \exp(i\Delta) = \frac{N_x \cos\theta - \epsilon_y \cos\theta + N_z \epsilon_z}{N_x \cos\theta + \epsilon_y \cos\theta - N_z \epsilon_z}$$

where $\epsilon = (1 - \sin^2\theta/N^2)^{1/2}$. Trial calculations have shown that when $n^2 + k^2 > 30$, ϵ could be taken as 1 and the calculations become considerably simpli-

fied.

Rapp measured the parameters of the elliptic reflected light (phase difference Δ and azimuth ψ) at high angles of incidence ϕ ($\phi = 75^\circ$ for wavelengths smaller than $1 \mu\text{m}$ and $\phi = 85^\circ$ for wavelengths larger than $1 \mu\text{m}$). He calculated the values of the complex refractive index along one crystallographic axis according to the formula

$$(n_1 - ik_1)^{-1} = \frac{\cos\phi}{1 - \cos^2\phi} \left(\frac{\cos 2\psi_1 + i \sin 2\psi_1 \sin\delta_1}{1 + \sin 2\psi_1 \cos\delta_1} + \cos^2\phi \frac{\cos 2\psi_2 + i \sin 2\psi_2 \sin\delta_2}{1 + \sin 2\psi_2 \cos\delta_2} \right)$$

which can be simplified when $\cos^2\phi \ll 1$ writing in the second term, which then plays a minor role, ψ_1 and δ_1 in the place of ψ_2 and δ_2 . Rapp noticed a difference of 1% between the two formulas for wavelengths larger than $1 \mu\text{m}$ and between 1% and 10% otherwise.

In view of our results we chose to calculate the

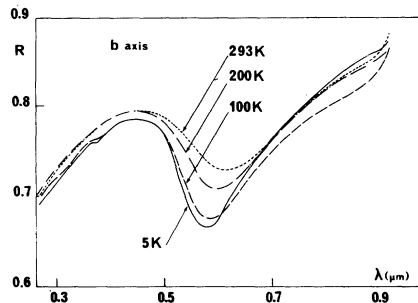


FIG. 5. Reflectance of a (001) surface, light polarized parallel to axis *b*, at different temperatures.

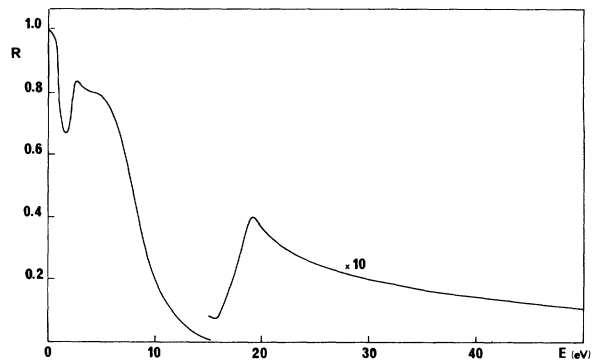


FIG. 7. Reflectance of a (001) surface, unpolarized light, up to 50 eV.

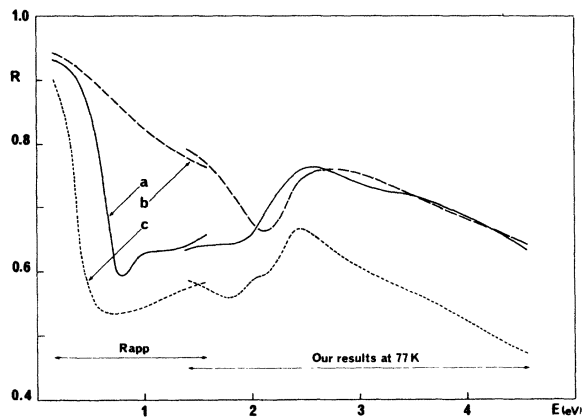


FIG. 8. Reflectance in the ir calculated from Rapp results and our results in the visible.

Ga optical constants using Kramers-Kronig analysis. This method requires knowledge of reflectance over an energy range as wide as possible. Reflectance measurements at normal incidence, with natural light, of a (001) face of a monocrystal, in the range 0.5–50 eV, show that reflectance falls to 1% at 15 eV and stays low for higher energies (Fig. 7).

Our experimental results have been extrapolated towards the high-energy side in order to have the same rate of decrease. On the low-energy side, we have calculated the values of reflectance at normal incidence using the indices determined by ellipsometry by Rapp. Figure 8 shows on one side the results of such a calculation in the ir and on the other side our experimental results.

It can be seen that there is a good agreement for the *a* and *b* axes, but it is less satisfactory for the *c* axis. This is rather general: Results concerning the *c* axis are usually less satisfactory

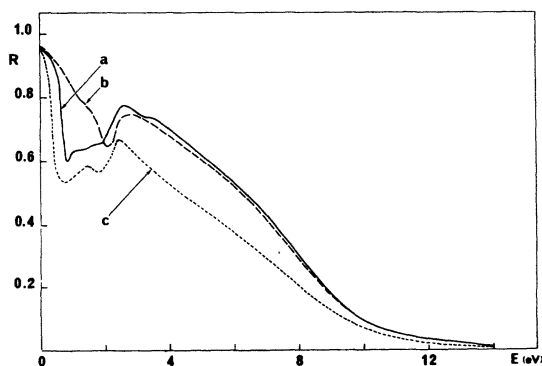


FIG. 9. *R* values used in order to calculate the dielectric constants.

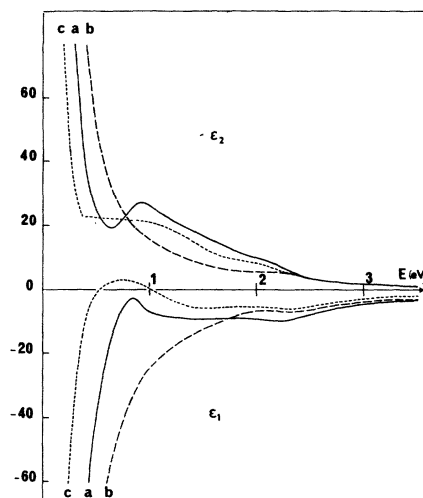


FIG. 10. Real ϵ_1 and imaginary ϵ_2 part of the dielectric constants along the three axes.

than those concerning the other two axes. This is due to the fact that it is very difficult to obtain a (010) face large and flat enough, when the crystal grows, in order to have good results concerning axis *c* ([001]) which stands in that face. Figure 9 gives *R* values which we used to determine the real ϵ_1 and imaginary ϵ_2 part of the dielectric constant relative to each crystallographic axis through Kramers-Kronig analysis. Figure 10 gives the values of ϵ_1 and ϵ_2 relative to the three axes while Figs. 11, 12, 13 give the values of ϵ_2 as determined by Rapp, Lenham, and Hunderi and Ryberg, respectively. The last workers have used films.

On these figures a Drude comportment can be seen on the low-energy side, being more important

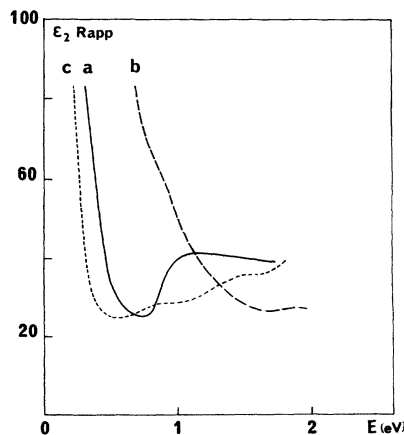


FIG. 11. Imaginary part of the dielectric constant calculated by Rapp.

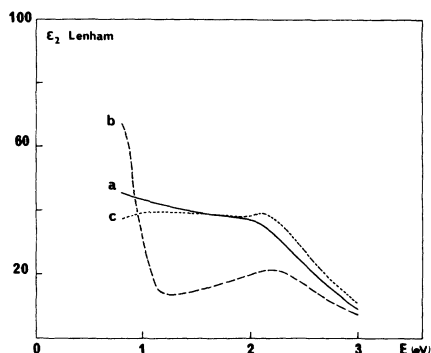


FIG. 12. Imaginary part of the dielectric constant calculated by Lenham.

for the b axis than for the a and c axes in all cases. However, Lenham⁹ showed that the data cannot be discussed in terms of simple free-electron theory. Band-structure calculations (cf. Sec. IV) show that band to band transitions may occur in the ir. In the visible the absorption bands are large and smooth so it is not possible to interpret the optical properties from static measurements. Figure 14 shows the imaginary part of $1/\epsilon$ pointing out that the plasma frequency occurs near 8 eV which is smaller than the earlier value^{13,14} of 10 eV.

III. THERMOREFLECTANCE

A. Measurements

Thermoreflectance spectra of Ga monocrystals have been investigated in two different ways.

First, slabs whose dimensions were $12 \times 4 \text{ mm}^2$, $15 \mu\text{m}$ thick had been prepared by mechanical grinding and polishing. A proper technique was used in order to avoid heating of the slabs and oxidizing. The faces of the slabs contained two

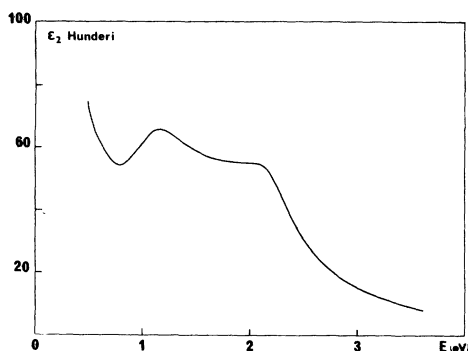


FIG. 13. Imaginary part of the dielectric constant calculated by Hunderi and Ryberg from measurements on films.

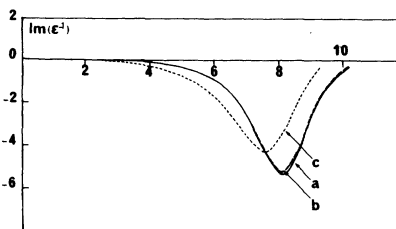


FIG. 14. $\text{Im}(1/\epsilon)$ vs energy.

crystallographic axes, which was checked with x rays. The slabs were then fixed onto the cold finger of a cryostat in order to work at different temperatures. A square-wave electric current flowed through them, whose frequency was 16 Hz. The maximum power dissipated was about 1 W which corresponds to a temperature modulation of about 1 K. The size of the slabs was chosen so that its electrical resistance would have a correct value. The monochromatic light beam fell on the free face of the sample at near normal incidence and was polarized parallel to a crystallographic axis. The reflected light modulated at the same frequency was detected with a lock-in amplifier. The relative change $\Delta R/R$ of the reflectance was registered. Measurements were made in the range 1.5–5 eV. A more detailed description of the apparatus is given in Ref. 15. Figures 15 and 16 show the thermoreflectance spectra at different temperatures for light polarized parallel to b axis and c axis, respectively. They show a shift towards lower energies as the mean temperature increases.

Another technique¹⁶ used a modulated electron beam in order to modulate the temperature of the samples. The slabs were $100 \mu\text{m}$ thick and they were cooled to liquid-nitrogen temperature. The measurements were made in the range 0.3–3 eV. Figure 17 shows on its upper part thermoreflect-

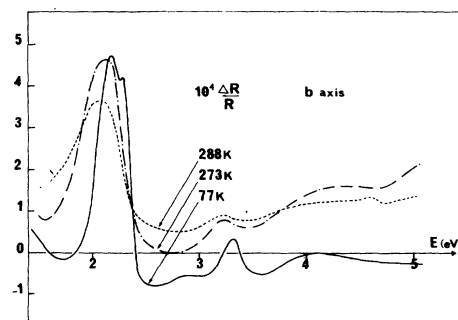


FIG. 15. Thermoreflectance spectra of gallium, light polarized parallel to axis b at different temperatures.

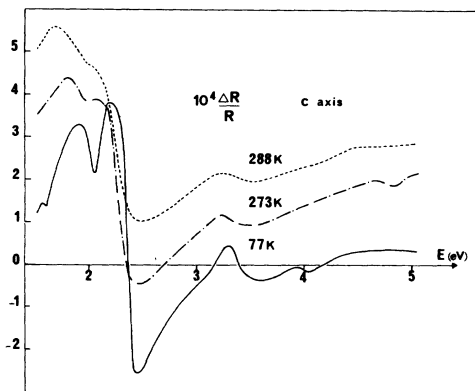


FIG. 16. Thermoreflectance spectra of gallium light polarized parallel to axis c at different temperatures.

ance spectra, for each crystallographic axis, obtained with this procedure, and, in its lower part, in view of comparison the results obtained with the first procedure. A good agreement is found in the common part of energy range.

B. Determination of the changes $\Delta\epsilon_1$ and $\Delta\epsilon_2$

A change Δt of the temperature of a sample produces a change $\Delta\epsilon_1$ in the real part of the dielectric constant and $\Delta\epsilon_2$ in its imaginary part. It can be shown¹⁷ that $\Delta\epsilon_1$ and $\Delta\epsilon_2$ are given functions of the relative change $\Delta R/R$ of the reflectance and of the phase change $\Delta\theta$ of the reflectivity ($r = R^{1/2} \exp j\theta$)

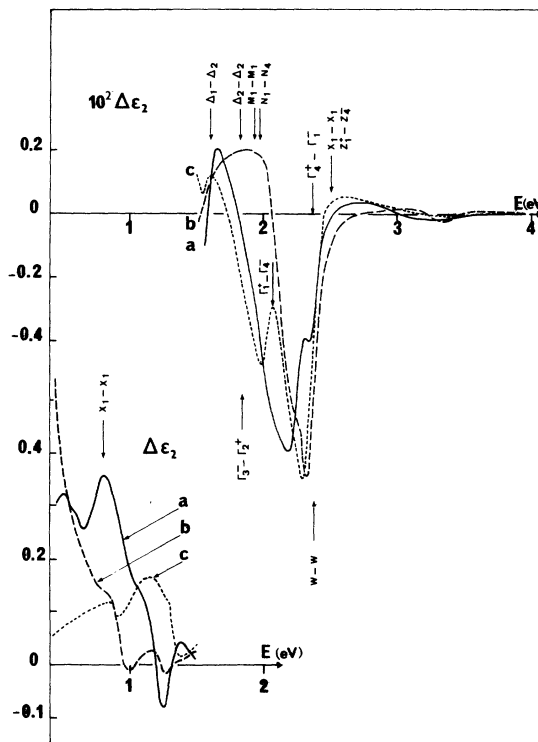


FIG. 18. Changes $\Delta\epsilon_2$ in the imaginary part of the dielectric constant corresponding to the three axes and transitions allowed.

$$\Delta\epsilon_1 = \frac{1}{2} \gamma \Delta R/R - \delta \Delta\theta,$$

$$\Delta\epsilon_2 = \frac{1}{2} \delta \Delta R/R + \gamma \Delta\theta,$$

where

$$\gamma = (\nu/n_0)(\nu^2 - 3\kappa^2 - n_0^2),$$

$$\delta = (\kappa/n_0)(3\nu^2 - \kappa^2 - n_0^2),$$

n_0 being the index of the medium in which stands the sample and ν and κ the sample indices. $\Delta\theta$ is determined through Kramers-Kronig analysis of $\Delta R/R$. Here each optical characteristic is referred to a crystallographic axis. Figure 18 is a plot of the changes in $\Delta\epsilon_2$ for each crystallographic axis which correspond to the first experimental method (upper part) and second experimental method (lower part). A strong anisotropy can be seen for energies lower than 2 eV, while the strong negative peak at 2.2–2.4 eV seems to be nearly the same for the three polarizations.

IV. INTERPRETATION OF THE RESULTS

It is known that optical spectra may be interpreted via electronic band structure. However the spectra obtained through static measurements are wide and smooth and correspond, for each

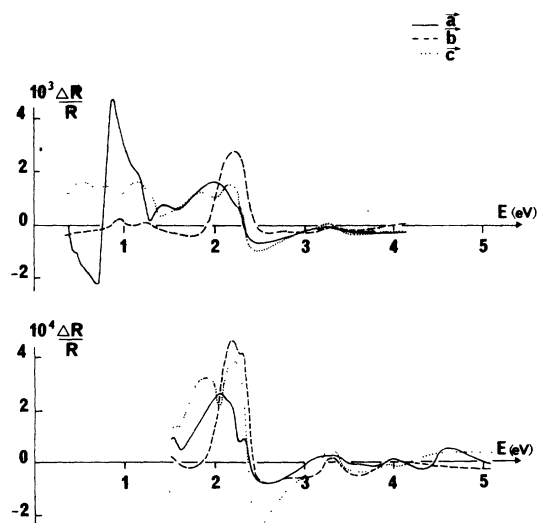


FIG. 17. Thermoreflectance spectra light polarized parallel to axis a , b , and c in the ir (upper part) and the visible (lower part).

photon energy, to transitions happening at all the points belonging to the same equal energy difference surface in momentum space. Those obtained through modulation spectroscopy, on the contrary, are usually sharp and well defined and may allow a better interpretation.

Thermoreflectance spectra of metals may be due to transitions at critical points, plasma resonance, transitions to or from Fermi level and intraband transitions (free-electron absorbance).¹⁸ When the temperature is modulated, the Fermi-Dirac distribution function is modulated near the Fermi level and a very narrow spectrum ($\sim kT$) may happen. We do not think that any structure in our thermoreflectance spectra could be due to such a modulation as our spectra are not sharp enough. Plasma resonance give peaks in $\Delta R/R$ having the same shape as functions β_1 and β_2 which appear in the expression of $\Delta R/R$ as a function of $\Delta\epsilon_1$ and $\Delta\epsilon_2$:

$$\Delta R/R = \beta_1 \Delta\epsilon_1 + \beta_2 \Delta\epsilon_2.$$

β_1 and β_2 are well behaved in the range of energy we investigate. Furthermore the dependence of $\text{Im}(\epsilon^{-1})$ (Fig. 14) shows that the plasma frequency occurs at energies higher than those we are investigating. We are then left with transitions at critical points and intraband transitions.

A change in the temperature has two consequences in the vicinity of a critical point: a shift of the gap ω_g and a change of the broadening parameter η . The temperature modulation of the optical constants related to the shift of ω_g is larger than that caused by broadening¹⁸ and has the same type of singularity as wavelength modulation since

$$\left(\frac{\partial \epsilon}{\partial T}\right)_{\eta=\text{const}} = -\frac{\partial \epsilon}{\partial \omega} \frac{\partial \omega_g}{\partial T}$$

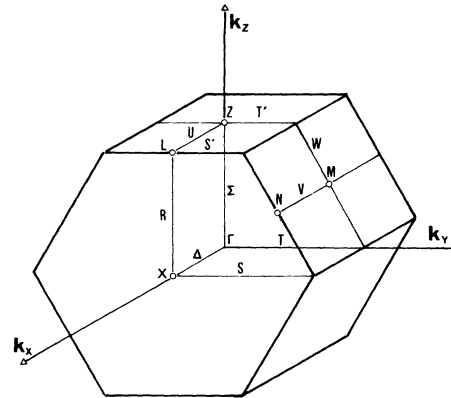


FIG. 19. Brillouin zone of gallium.

and $\epsilon \sim (\omega - \omega_g)^{+1/2}$. $\partial \omega_g / \partial T$ is negative as can be seen on the shifts of thermoreflectance spectra at different temperatures (Figs. 15 and 16). The shape of the changes in $\Delta\epsilon_1$ and $\Delta\epsilon_2$ are then given by a universal function $F((\omega - \omega_g)/\eta)$.^{18,19} The amplitude of these changes, however, depends on the product $a_x a_y a_z$ of the coefficients in the expression of the energy difference between two bands in the vicinity of a critical point as a function of wave vector

$$\omega = \omega_g + a_x k_x^2 + a_y k_y^2 + a_z k_z^2.$$

The smaller the product, the higher is $\Delta\epsilon$. The critical point investigated is a M_0 , M_1 , M_2 , or M_3 point according to the number of negative values taken by a_x , a_y , a_z . Finally, this amplitude depends on the value of the matrix element of the transition, some of them being certainly zero, which can be seen using group theory. Characters of operations in the group of the wave vector at different points

TABLE I. Principal transitions relative to critical points corresponding to different energy bands.

ΔE (eV)	Transition	E_i (eV)	E_f (eV)	Critical point	Polarization
0.8	$X_1 \rightarrow X_1$	9.42	10.23	M_0 and M_1	a, c
1.64 ^a	$\Delta_1 \rightarrow \Delta_2$			M_1	c
1.82 ^a	$\Delta_2 \rightarrow \Delta_2$			M_0	c
1.84	$\Gamma_3^- \rightarrow \Gamma_2^+$	8.51	10.35	M_2	c
1.93	$M_1 \rightarrow M_1$	8.45	10.38	M_0	a, b, c
1.97	$N_1 \rightarrow N_4$	8.11	10.08	M_0	a, b, c
2.08	$\Gamma_1^+ \rightarrow \Gamma_1^-$	8.65	10.73	M_0	c
2.11	$Z_3^- \rightarrow Z_2^+$	8.32	10.43	M_1	c
2.36	$\Gamma_4^+ \rightarrow \Gamma_1^-$	8.11	10.47	M_1	c
2.38 ^a	$W \rightarrow W$			M_3	a, b, c
2.49	$X_1 \rightarrow X_1$	9.42	11.91	M_0 and M_1	a, c
2.52	$Z_1^+ \rightarrow Z_4^-$	8.16	10.68	M_1	c

^aThese values have been estimated after interpolation.

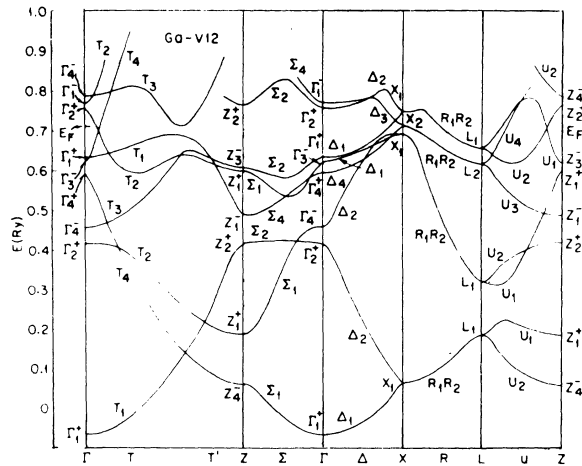


FIG. 20. Band structure of gallium according to Reed.

of the Brillouin zone (Fig. 19) have been evaluated by Slater *et al.*⁷ Band calculations have been made by these authors using the free-electron approximation while Reed²⁰ and, recently, Hunderi and Ryberg,⁶ used a pseudopotential method. The results of Hunderi and Ryberg are quite similar to those of Reed but they give in addition energy bands along Γ - M and W and matrix elements at some important symmetry points: Γ , Z , and M .

Our thermorefectance spectra show important structures for energies lower than 3 eV. Table I shows the principal transitions which are not forbidden by group theory relative to the critical points which have been found from the values of energy bands evaluated by Reed. The first column shows the energy of the transition, the second gives the transition, the third and fourth the energy of the initial and final value of the electron energy, the fifth the nature of the critical point, and the sixth the polarization of the light for which the transition is not forbidden. Figure 20 shows the band structure along some symmetry directions.

It shows that there is no selection rule for transitions at M , N , and W , and these transitions are the only ones found when light is polarized parallel to b axis. We think therefore that the positive peak of $\Delta\epsilon_2$ (Fig. 18 curve b) between 1.6 and 2 eV must be attributed to transitions at M and N while the negative peak at 2.31 eV must be attributed to transition at W . Such a negative peak is also found for the other two polarizations at nearly the same energy and is certainly related to the same transition. The transitions at M and

N do not appear for light polarized parallel to a and c axes but this should be attributed to the fact that other transitions occur in this range of energy and that the matrix elements for these transitions could be larger. For example, Hunderi and Ryberg have found that the matrix elements are 0.4 at M and 1.83 for the transition $\Gamma_1^+ \rightarrow \Gamma_4^-$ (at 2.19 eV according to them and at 2.08 eV according to Reed), which makes this transition twenty times larger, other things equal. According to these remarks the peaks in $\Delta\epsilon_2$ can be attributed to characteristic transitions which are indicated by arrows in Fig. 18.

When free-electron absorption is taken into account, $\Delta\epsilon_2$ is increasing with light wavelength. Such a contribution can only be seen on the low-energy side for light polarized parallel to b axis. Such a Drude comportment is also seen on static measurements of ϵ . These experimental results and band-structure calculations suggest that transitions should occur for energies lower than 0.3 eV and such a range should be investigated.

CONCLUSION

Reflectance measurements, at normal incidence, light being polarized parallel to each crystallographic axis of natural gallium monocrystal surfaces have been made. The optical constants relative to each axis have been determined through Kramers-Kronig analysis. These results show that gallium is strongly anisotropic and in order to interpret them, we report on thermorefectance spectra from which the changes $\Delta\epsilon_2$ in the imaginary part of the three dielectric constants have been determined. These spectra are strongly anisotropic and can be interpreted with the aid of band structure and selection rules. These results show that for energies lower than 0.3 eV, interband transitions should be expected and that Drude comportment can be seen down to 0.3 eV only with light polarized parallel to the b axis.

ACKNOWLEDGMENTS

The authors thank Professor Hanus, Dr. Debever and Dr. Humbert, groupe de Physique des États Condensés Marseille Luminy (France), who measured thermorefectance spectra in the ir and Dr. Ferraton and Dr. Ance, Laboratoire Spectroscopie II Université des Sciences et Techniques Montpellier (France), who measured reflectances in the uv.

- ¹C. Wesolowska, *Acta Phys. Pol.* XXV, 323 (1964).
²C. Wesolowska, E. Dobierzewska-Mozrzymasova, and B. Jakubowsky, *Acta Phys. Pol.* XXV, 443 (1964).
³I. Yu Rapp, I. N. Shklyarevskii, and R. G. Yarovaya, *Fiz. Tverd. Tela* 10, 2257 (1968).
⁴J. Bor, and C. Bartholomew, *Proc. Phys. Soc.* 90, 1153 (1967).
⁵A. Yu Eichis and G. P. Skorniyakov, *Opt. Spectrosc.* 16, 86 (1964).
⁶O. Hunderi and R. Ryberg, *J. Phys. F* 4, 2084 (1974).
⁷J. C. Slater, G. F. Koster and J. H. Wood, *Phys. Rev.* 126, 1307 (1962).
⁸A. P. Lenham, *Proc. Phys. Soc.* 82, 933 (1963).
⁹A. P. Lenham and D. M. Treherne, *J. Opt. Soc. Am.* 56, 752 (1966).
¹⁰I. Yu. Rapp, R. G. Yarovaya, and L. A. Bondarenko, *Fiz. Met. Metalloved.* 32, 728 (1971).
¹¹J. R. Beattie, *Philos. Mag.* 46, 238 (1955).
¹²P. Drude, *Wied. Ann. Phys.* 32, 623 (1887).
¹³J. P. Ferraton, C. Ance, R. Kofman, P. Cheyssac, and J. Richard, *C. R. Acad. Sci. B* 283, 253 (1976).
¹⁴J. L. Robins, *Proc. Phys. Soc.* 79, 119 (1962).
¹⁵A. Jolivet, R. Garrigos, and R. Kofman, *Rev. Phys. Appl.* 7, 403 (1972).
¹⁶H. Dallaporta, J. M. Debever, and J. Hanus, *J. Phys. Lett.* 37, 139 (1976).
¹⁷B. O. Seraphin, *Semiconductors and Semimetals*, Vol. 9 (Academic, New York and London, 1972).
¹⁸M. Cardona, *Modulation Spectroscopy Solid State Physics II* (Academic, New York, 1969).
¹⁹B. Batz, Ph.D. thesis (Univ. libre de Bruxelles, 1967).
²⁰W. A. Reed, *Phys. Rev.* 188, 1184 (1969).

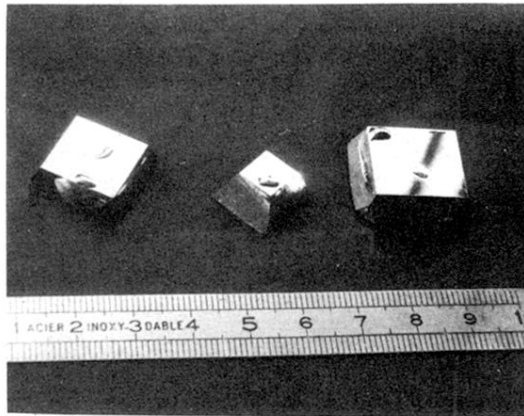


FIG. 2. Photography of gallium monocrystals.